Geofluids (2007) 7, 79–95 doi: 10.1111/j.1468-8123.2006.00165.x

Numerical modeling of the origin of calcite mineralization in the Refugio-Carneros fault, Santa Barbara Basin, California

M. S. APPOLD[1], G. GARVEN[2], J. R. BOLES[3] AND P. EICHHUBL[4]

[1]Department of Geological Sciences, University of Missouri-Columbia, Columbia, MO, USA; [2]Department of Earth & Planetary Sciences, Johns Hopkins University, Baltimore, MD, USA; [3]Department of Geological Sciences, University of California-Santa Barbara, Santa Barbara, CA, USA; [4]Bureau of Economic Geology, The University of Texas at Austin, Austin, TX, USA

ABSTRACT

Many faults in active and exhumed hydrocarbon-generating basins are characterized by thick deposits of carbonate fault cement of limited vertical and horizontal extent. Based on fluid inclusion and stable isotope characteristics, these deposits have been attributed to upward flow of formation water and hydrocarbons. The present study sought to test this hypothesis by using numerical reactive transport modeling to investigate the origin of calcite cements in the Refugio-Carneros fault located on the northern flank of the Santa Barbara Basin of southern California. Previous research has shown this calcite to have low $\delta^{13}C$ values of about −40 to −30‰ PDB, suggesting that methane-rich fluids ascended the fault and contributed carbon for the mineralization. Fluid inclusion homogenization temperatures of 80–125°C in the calcite indicate that the fluids also transported significant quantities of heat. Fluid inclusion salinities ranging from fresh water to seawater values and the proximity of the Refugio-Carneros fault to a zone of groundwater recharge in the Santa Ynez Mountains suggest that calcite precipitation in the fault may have been induced by the oxidation of methane-rich basinal fluids by infiltrating meteoric fluids descending steeply dipping sedimentary layers on the northern basin flank. This oxidation could have occurred via at least two different mixing scenarios. In the first, overpressures in the central part of the basin may have driven methane-rich formation waters derived from the Monterey Formation northward toward the basin flanks where they mixed with meteoric water descending from the Santa Ynez Mountains and diverted upward through the Refugio-Carneros fault. In the second scenario, methane-rich fluids sourced from deeper Paleogene sediments would have been driven upward by overpressures generated in the fault zones because of deformation, pressure solution, and flow, and released during fault rupture, ultimately mixing with meteoric water at shallow depth. The models in the present study were designed to test this second scenario, and show that in order for the observed fluid inclusion temperatures to be reached within 200 m of the surface, moderate overpressures and high permeabilities were required in the fault zone. Sudden release of overpressure may have been triggered by earthquakes and led to transient pulses of accelerated fluid flow and heat transport along faults, most likely on the order of tens to hundreds of years in duration. While the models also showed that methane-rich fluids ascending the Refugio-Carneros fault could be oxidized by meteoric water traversing the Vaqueros Sandstone to form calcite, they raised doubts about whether the length of time and the number of fault pulses needed for mineralization by the fault overpressuring mechanism were too high given existing geologic constraints.

Key words: fault, methane, modeling, overpressure, Santa Barbara

Received 7 December 2005; accepted 22 September 2006

Corresponding author: M. S. Appold, Department of Geological Sciences, University of Missouri–Columbia, Columbia, MO 65211, USA.
Email: appoldm@missouri.edu. Tel: 573 882 0701. Fax: 573 882 5458.

INTRODUCTION

The Santa Barbara Basin is an approximately 100 km-long sedimentary trough that originated from transpression of the southern California continental margin beginning in the late Oligocene (Fig. 1). The basin has been geologically very active throughout its brief history, and is important as a laboratory for modern marine tectonic and sedimentary processes, as well as for the commercial production of hydrocarbons. Significant accumulations of hydrocarbons occur throughout the Tertiary stratigraphic section leading to a total resource endowment – the sum of cumulative production, proven reserves, and probable undiscovered reserves – of about 3 billion barrels of oil and 7 trillion cubic feet of natural gas (Galloway 1998), with the greatest concentrations occurring in the Miocene-age Monterey Formation (Fig. 2). Recent to modern hydrocarbon seeps, manifest as active gas vents, mats of sulfide oxidizing bacteria, and authigenic carbonate cements are common in the geographic center of the basin where subsidence, burial, and diagenesis are ongoing, and along the basin's northern flank (Eichhubl *et al.* 2000; Boles *et al.* 2001). The seeps are strongly controlled by faults and fractures that serve as conduits through low permeability fine-grained clastic units prevalent in the basin (Eichhubl & Behl 1998; Eichhubl *et al.* 2000).

A prominent example of recent (as young as Quaternary) hydrocarbon seepage in the Santa Barbara Basin occurs as extensive calcite cements as much as 1.5 m thick at the ends of the Refugio-Carneros fault, an approximately 24-km long WNW-ESE trending fault on the northern margin of the basin (Fig. 1). The Refugio-Carneros fault is one of several similarly trending faults on the basin's coastal margin that together reflect a clockwise shift along the Pacific and North American plate junction since the Miocene (Nicholson *et al.* 1994). Boles & Grivetti (2000) and Boles *et al.* (2004) have studied the calcite cementation in the Refugio-Carneros fault and provide important insights into the calcite's origin and more broadly into the fluid history of the Santa Barbara Basin. Their work showed that carbon in the calcite cements was probably derived from methane, based on low $\delta^{13}C$ values clustered predominantly between about −30 and −40‰ (PDB). They suggested that the cementation was likely contemporaneous with faulting based on the cement's brecciation, slickensides, and pervasive lamellar twinning. U-Th dating of calcite indicates that this cementation may have occurred as recently as 107 000–420 000 years ago, though a second set of samples yielded apparent ages older than the 500 000 year maximum limit of applicability of the U-Th dating technique. Fluid inclusion homogenization data indicate minimum temperatures of calcite precipitation of about 80–125°C. Because the calcite deposition was relatively recent and was probably never deeply buried (Boles & Grivetti 2000), these temperatures indicate rapid fluid flow and heat transport up the fault. Fluid inclusion last ice melting temperatures indicate a range of salinities from about 0.3 to 3.5 equivalent weight percent NaCl. Together with low overall trace element concentrations compared to pore-filling calcite cements formed at similar temperatures and burial diagenetic settings, these data suggest mixing between a saline basinal fluid and a dilute, possibly meteoric fluid.

The results of Boles & Grivetti (2000) and Boles *et al.* (2004) suggest a scenario for the origin of the calcite cements in the Refugio-Carneros fault in which saline,

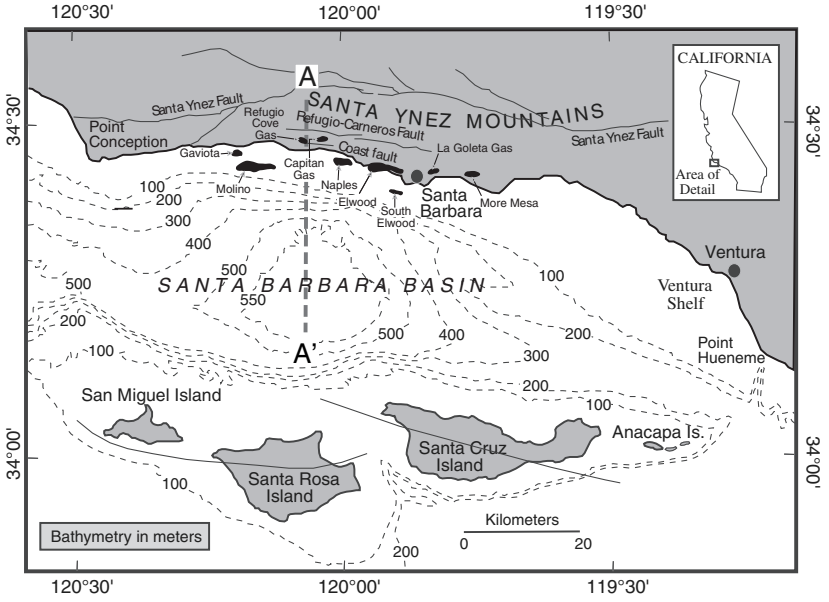

Fig. 1. Location map and bathymetry of the Santa Barbara Basin (after Reimers *et al.* 1996). The bold dashed line A–A′ is the surface trace of the profile used in the numerical modeling. Bathymetry contours are shown as narrow dashed lines. Faults are shown as solid lines. The Refugio-Carneros and Coast faults and major nearby hydrocarbon fields are labeled.

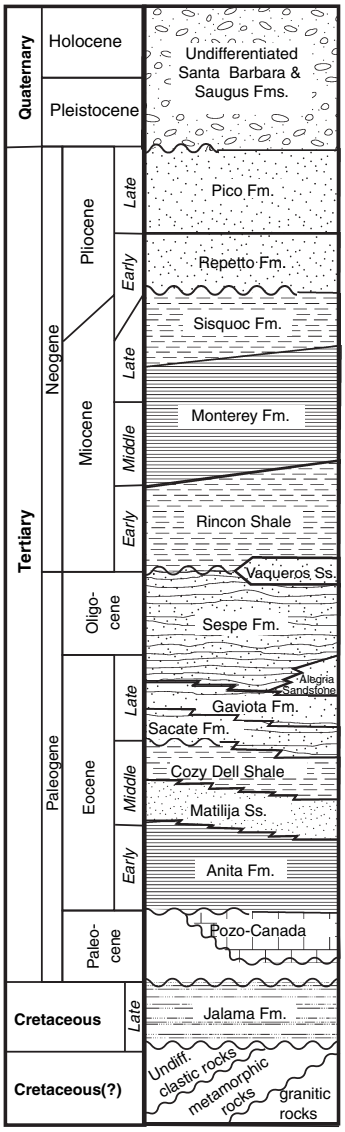

Fig. 2. Generalized stratigraphy of the Santa Barbara Basin (after Galloway 1998).

reducing, methane-rich fluids ascended the fault from deeper parts of the basin and mixed with dilute, oxidizing, meteoric fluids descending from a recharge zone in the Santa Ynez Mountains. The Vaqueros Sandstone may have been a particularly important conduit for this meteoric fluid based on its high present-day permeability (Briggs 2003) and the fact that the calcite mineralization occurs at the intersection of the Refugio-Carneros fault with the Vaqueros. At least two manifestations of this mixing scenario can be postulated. In the first, overpressures in the central part of the basin may have driven methane-rich formation waters derived from the Monterey Formation northward toward the basin flanks where they mixed with meteoric water descending from the Santa Ynez Mountains through steeply dipping aquifers and diverted upward through the Refugio-Carneros fault. Boles *et al.* (2004) began testing this first scenario with numerical fluid flow and heat transport modeling, showing that if the submarine portion of the Santa Barbara Basin had reached overpressures on the order of 80% of lithostatic, a thermal transient with duration on the order of 10^3 years could have been produced once the fault became conductive to fluid flow, and with temperatures similar to the fluid inclusion homogenization temperatures at depths as shallow as 300 m. In the second scenario, methane-rich fluids sourced from deeper Paleogene sediments would have been driven upward by overpressures generated in the fault zones because of deformation, pressure solution, and flow (Gratier *et al.* 2002, 2003), and released during fault rupture, ultimately mixing with meteoric water at shallow depth. The focus of the present study was on this second scenario, and treated the effects not only of fluid flow and heat transport considered by Boles *et al.* (2004) but also reactive solute transport. The incorporation in the current models of reactive solute transport had the benefit of allowing the response of calcite precipitation to changing solute and heat fluxes to be tested directly. In short, the study sought to quantify the relative contributions of topography and fault overpressuring as fluid-driving mechanisms in the basin, the conditions needed for apparent calcite mineralization temperatures to be reached in the upper parts of the Refugio-Carneros fault, and the spatial distribution and mass of calcite mineralization produced by mixing of oxidizing meteoric groundwater with methane-rich basinal fluids derived from deep hydrocarbon reservoirs or source rocks in the basin.

GEOLOGIC BACKGROUND

The Santa Barbara Basin is located at the northern end of the California continental borderland, a region of irregular shelf morphology extending from Isla Cedros off Baja California to Point Arguello in southern California (Gorsline & Teng 1989). The Santa Barbara Basin is one of about two dozen sedimentary basins in this region that formed as a result of a progressive shift beginning in the Late Mesozoic from high angle subduction to transform slip, with the resulting crustal rotation largely responsible for bringing about the opening of the basins (Crouch 1979; Howell *et al.* 1980; Hornafius *et al.* 1986; Gorsline & Teng 1989). The oldest sedimentary rocks in the Santa Barbara Basin belong to the Upper Cretaceous Jalama Formation and consist of marine mudstones and sandstones deposited in a forearc setting (Galloway 1998). This tectonic environment and the deposition of similar lithologies persisted until the Oligocene, producing an aggregate thickness of sediment approaching as much as 6 km (Tennyson & Isaacs 2001). During the Miocene, the crust in the Santa Barbara Basin region was rotated 90° clockwise to its

present east–west trending configuration (Hornafius *et al.* 1986). Rapid subsidence and sedimentation continued, leading to the accumulation of perhaps another 5 km of sediment from the Miocene to the present day (Tennyson & Isaacs 2001). Sedimentation during this time interval still consisted predominantly of fine-grained clastics, but with a significant proportion of sandstones and conglomerates caused by the emergence and weathering of topographic highs created as a result of the crustal rotation. Further products of this crustal rotation are the formation of several west–east- to northwest–southeast-trending faults in the Santa Barbara coastal area and the uplift of the Santa Ynez Mountains, which form the northern margin of the Santa Barbara Basin, by Pliocene time (Jackson & Yeats 1982).

The Refugio-Carneros fault is an example of one of these faults and has been described by Boles & Grivetti (2000) and Boles *et al.* (2004), from which the following summary is based. The fault crops out intermittently over a 24-km length in Oligocene–Miocene Vaqueros Sandstone and Miocene Rincon Shale, and may penetrate to several kilometers depth at a northward dip ranging from 35° to 60°. Coarsely crystalline calcite cement occurs as tabular bodies and is limited to the western and eastern ends of the fault, perhaps because these regions experienced the greatest dilation and therefore would have allowed the highest fluxes of fluid. High fluid fluxes may also have made it possible to transport the heavy mineral and quartz sand grains that occur as detrital layers in the growth bands of many radiating crystals of calcite. Acicular sprays of these crystals that nucleated on the walls of veins and grew inward to lengths as great as 10 cm indicate that the rate of fracture opening was greater than that of crystal growth, and that the fault may have had a relatively large aperture, which would have promoted rapid fluid flow. Some of the calcite in the fault as well as sandstone country rock adjacent to the fault contains abundant hematite, whereas sandstone farther from the fault contains pyrite and only sparse hematite. These observations indicate the presence of oxidizing fluids within the fault zone, and support the hypothesis that calcite occurring there originated by oxidation of methane. The observations also suggest that if meteoric water descended through the Vaqueros Sandstone, a hypothesis considered in the current study, flow may have been predominantly through fractures and bedding plane partings to prevent pyrite in the matrix from becoming oxidized.

Hydrocarbon generation has occurred during much of the history of the Santa Barbara Basin, with major fields reported for strata ranging from the Cretaceous Jalama Formation to the Late Pliocene Pico Formation (Galloway 1998). The Miocene Monterey Formation is widely considered to be the most important source of hydrocarbons in the basin, though smaller amounts may also have been contributed from other formations. Most of the larger hydrocarbon accumulations occur in anticlinal traps, commonly bounded on at least one side by steeply dipping reverse faults (Nagle & Parker 1971; Keller 1990; Tennyson & Isaacs 2001). Major hydrocarbon fields presently located near the Refugio-Carneros fault and the stratigraphic unit in which they occur (parentheses) include the Gaviota (Sespe-Vaqueros), Molino (Monterey), Refugio Cove (Sespe-Vaqueros), Capitan (Sespe-Vaqueros), Naples (Vaqueros), Ellwood (Upper Sespe-Vaqueros-Rincon), La Goleta (Vaqueros), and More Mesa (Vaqueros; Fig. 1; Giallonardo & Koller 1978; Boles *et al.* 2004). Any one of these fields would have had sufficient methane to account for the calcite contained within the Refugio-Carneros fault. For example, a mass balance calculation by Boles & Grivetti (2000) shows that the carbon needed to form all of the calcite known from the western end of the fault could have been supplied from only 1% of the total methane formerly present in the now abandoned Refugio Cove field, the closest to the calcite mineralization.

MODEL DESIGN

Finite element numerical modeling of fluid flow, heat transport, and reactive solute transport was carried out on a grid (Fig. 3) based on the cross section shown in Fig. 4 using the program RST2D, developed and described by Raffensperger & Garven (1995a,b). To compute fluid flow, RST2D solves a mass balance equation of the form,

$$-\nabla \cdot (\rho \mathbf{q}) = \rho S_s \frac{\partial h}{\partial t} \tag{1}$$

in conjunction with a variable-density and viscosity form of Darcy's law,

$$\mathbf{q} = -\mathbf{K}\mu_r(\nabla h + \rho_r \nabla z). \tag{2}$$

In these equations, h is equivalent fresh water hydraulic head, $\mathbf{K}$ is the hydraulic conductivity tensor, $\mathbf{q}$ is the specific discharge, S_s is specific storage, t is time, z is elevation, ρ is fluid density at ambient conditions, ρ_r is relative fluid density, defined as

$$\rho_r = \frac{\rho - \rho_0}{\rho}, \tag{3}$$

where ρ_0 is a reference state density, and μ_r is a relative density defined as

$$\mu_r = \frac{\mu_0}{\mu}, \tag{4}$$

where μ_0 is a reference state viscosity, and μ is the viscosity at ambient conditions.

Heat transport is computed by RST2D via the following conservation of thermal energy equation:

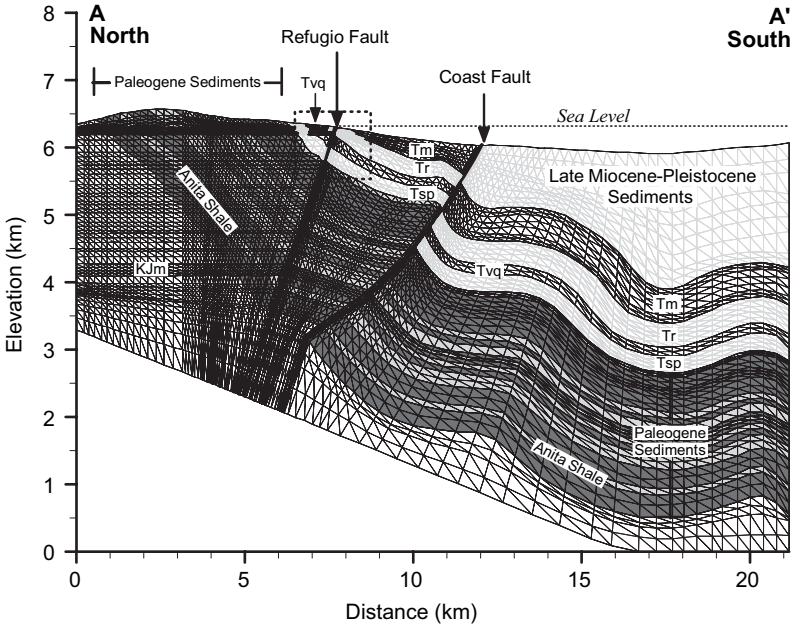

Fig. 3. Model numerical grid and hydrostratigraphy based on the cross section in Fig. 4. Dashed box near the top of the Refugio-Carneros fault shows the area represented by Fig. 12.

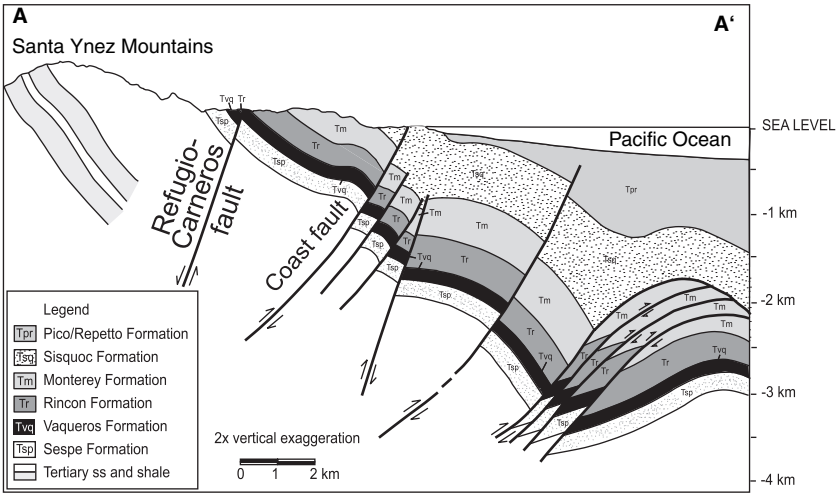

Fig. 4. Cross section of the north-central Santa-Barbara basin along the transect A–A′ (see Fig. 1) upon which the model hydrostratigraphy shown in Fig. 3 was based (after Boles *et al.* 2004).

$$\nabla \cdot (\lambda^* \nabla T) - \rho_f c_f \mathbf{q} \cdot \nabla T = (\rho c)_e \frac{\partial T}{\partial t}, \tag{5}$$

where c is the heat capacity, T is temperature, and λ^* is an effective thermal dispersion coefficient. The subscripts 'f' and 'e' refer to the fluid and effective saturated porous medium, respectively. Reactive solute transport is computed according to the equation:

$$\nabla \cdot (\Phi \mathbf{D} \nabla M^T_{c,aq}) - \Phi \mathbf{v} \cdot \nabla M^T_{c,aq} = \frac{\partial \Phi M^T_c}{\partial t}. \tag{6}$$

Here M^T_c is the total concentration in moles per cubic meter of bulk porous medium (mol m^{-3} BPM) of a component divided among all geochemical species, present in both the matrix and in the aqueous phase. The term $M^T_{c,aq}$ is the total concentration of a component in mol m^{-3} BPM divided only among aqueous species. **D** is the dispersion tensor, **v** is the average linear velocity, and Φ is porosity. Chemical reaction is computed according to equilibrium mass action equations:

$$K = \prod_i a_i^{\nu_i}, \tag{7}$$

where a_i is the activity of the ith species, ν_i is the stoichiometric reaction coefficient for the ith species, and K is the thermodynamic equilibrium constant. Reaction kinetics are not treated in the modeling, implying that the rate of reaction is fast compared to the rate of groundwater flow. Equation (7) is coupled to the solute transport Eqn (6)

through mineral precipitation or dissolution reactions that change the value of $M^T_{c,aq}$. Equilibrium constants were computed using the SUPCRT software and database (Johnson *et al.* 1992) for temperatures and pressures lying along the liquid–vapor equilibrium curve. Aqueous activity coefficients were computed using a high ionic strength form of the extended Debye-Hückel equation (Helgeson 1969). Changes in permeability as a function of changes in porosity due to mineral precipitation and dissolution were calculated using the empirical relationship of Walsh (1983):

$$\ln \frac{k}{k_0} = 45.7(\Phi - \Phi_0), \tag{8}$$

where Φ_i is the initial porosity and k_0 is the initial permeability.

The models in the present study were based on the cross section in Fig. 4, which shows the present-day geology along the transect A–A′ in Fig. 1 and intersects the western end of the Refugio-Carneros fault. The cross section was altered for the models so that steeply dipping units incompletely depicted in Fig. 4 were projected downward as far as the Coast fault at dips approximately parallel to shallower, more completely depicted units (Fig. 3). Complex and poorly understood structures south of the Coast fault were simplified and generalized as continuous folds. A further assumption of the modeling was that the coastline was further inland at the time of mineralization than at the present day, i.e., at about the location of the Refugio-Carneros fault instead of the Coast fault, because of ongoing uplift, though the precise location of the coastline at that time is uncertain.

Nine separate hydrogeologic units were considered in the model. The geology of these units has been described in numerous publications, including Hinman & Schwartz (1990), Tennyson & Kropp (1998), and Tennyson & Isaacs (2001). The lowermost unit in the model grid corresponds to the upper Jalama Formation, a unit of Cretaceous age abyssal shales and claystones, interbedded with minor thin sandstones. The Jalama Formation is overlain in the model by an Eocene–Oligocene sequence of alternating sandstones and shales that encompasses the Anita Formation, Matilija Sandstone, Cozy Dell Shale, Sacate Formation, Coldwater Sandstone, Gaviota Formation, and Alegria Formation. The next unit considered is the Sespe Formation, which consists of Oligocene alluvial sandstones, siltstones, and conglomerates. Overlying the Sespe is the Vaqueros Sandstone, a relatively thin formation of nearshore well cemented sandstones and conglomerates of latest Oligocene to earliest Miocene in age. The Lower Miocene Rincon Shale overlies the Vaqueros Sandstone and consists of mudstone, shale, and sandstone. Above the Rincon Shale is the Monterey Formation, a thick, mostly deep water sequence of shales, siliceous and calcareous mudstones, dolostones and limestones, and porcellanites and cherts, parts of which have been heavily fractured. The topmost unit considered in the model is a thick sequence of undifferentiated Late Miocene to Pleistocene sediments that includes the diatomaceous clay shales of the Sisquoc Formation, fine-grained sandstones and siltstones of the Repetto, Pico, and Santa Barbara formations, and gravel and pebbly sandstones of the Casitas Formation. The Refugio-Carneros and Coast faults in the models were treated as separate hydrogeologic units from the remaining units described above, each consisting of a 10- to 25-m wide steeply dipping high permeability conduit cutting across the basin. Thus, in the models, the faults were treated as high permeability fractured zones that were wider than the apertures of the Refugio-Carneros and Coast faults alone, which is supported by observations of calcite veins extending from the faults well into the adjacent country rock (Boles *et al.* 2004). Evidence for the relatively high permeability of these fault zones comes from the high fluid inclusion homogenization temperatures and detritus in the calcite cements noted previously (Boles & Grivetti 2000; Boles *et al.* 2004), features that are present in other faults in the area where high permeabilities have been documented (Eichhubl & Boles 2000a,b).

The values of major physical parameters used for the base case simulation are listed in Table 1. Constraints on the hydraulic conductivities of the major hydrostratigraphic units in the model were obtained from reports by Giallonardo & Koller (1978), Keller (1995), and Briggs (2003). Fault hydraulic conductivities were not included in these reports, so in the present models they were varied systematically as part of the sensitivity analysis. Porosity values for the Late Miocene–Pleistocene sediments and Monterey Formation were chosen from within the ranges reported by Keller (1995). For the remaining hydrogeologic units, porosity values were chosen from within the ranges for general lithologic type reported by Schwartz & Zhang (2003). Longitudinal solute dispersivity values of 100 m typical for flow at regional scales were chosen for most of the hydrogeologic units, with transverse values a factor of 10 lower (Gelhar *et al.* 1992). Thermal dispersivities were assumed to reflect solute dispersivities but to be isotropic. Matrix thermal conductivity values of 2.5 W m^{-1} K^{-1} were assigned to shale units and to the faults, and values of 3.5 W m^{-1} K^{-1} were assigned to sandstones (Blackwell & Steele 1989). Matrix compressibility values were chosen from within the range corresponding to consolidated rock, with the faults and younger Pliocene–Pleistocene sediments assumed to have values near the lower end of this range (Freeze & Cherry 1979). A specific heat value of 750 J kg^{-1} K^{-1} representative of sandstone and shale (Sabins 1997) was assigned to each hydrogeologic unit.

The models were designed to consider two major driving forces for fluid flow in the basin – (1) topographic

Table 1 Physical model parameters used for the base case simulation.

	Klm Jalama Fm	Eocene–Oligocene shales	Eocene–Oligocene sandstone	Tsp Sespe Fm	Tvq Vaqueros Sandstone	Tr Rincon Shale	Tm Monterey Fm	Late Miocene–Pleistocene sediments	Coast fault	Refugio-Carneros fault
K_x, Horizontal hydraulic conductivity (m year^{-1})	0.001	0.01	10	0.1	100	0.01	10	0.1	100 (open) 0.01 (sealed)	100 (open) 0.01 (sealed)
K_x/K_z, Horizontal: vertical ratio	100	100	100	100	100	100	100	10	1	1
Φ, Porosity (%)	10	15	20	20	20	15	25	30	10	10
α_L, Longitudinal dynamic dispersivity (m)	100	100	100	100	500	100	100	100	10	10
α_L/α_T, Longitudinal: transverse ratio	10	10	10	10	5	10	10	10	0.1	0.1
e_L, Longitudinal thermal dispersivity (m)	100	100	100	100	100	100	100	100	100	100
e_L/e_T, Longitudinal: transverse ratio	1	1	1	1	1	1	1	1	1	1
λ, Matrix thermal conductivity (W m^{-1} K^{-1})	2.5	2.5	3.5	3.5	3.5	2.5	3.0	3.0	2.5	2.5
α, Matrix compressibility (Pa^{-1})	3×10^{-10}	3×10^{-10}	3×10^{-10}	3×10^{-10}	3×10^{-10}	3×10^{-10}	3×10^{-10}	3×10^{-9}	3×10^{-9}	3×10^{-9}
c, Specific heat of matrix (J kg^{-1} K^{-1})	750	750	750	750	750	750	750	750	750	850

gradients from the Santa Ynez Mountains to the coastline and (2) overpressures developed in the Refugio-Carneros and Coast faults due to their hydraulic connection to higher pressure fluids deeper in the crust, or crack sealing by pressure solution and compaction of low permeability fault gouge during fault compression (Byerlee 1990, 1993; Rice 1992; Sleep & Blanpied 1992; Gratier *et al.* 2002, 2003). The models assumed an initially conductive temperature profile throughout the basin. The models also assumed initially hydrostatic conditions throughout the basin, except in the Refugio-Carneros and Coast fault zones, which were overpressured by up to 80% of lithostatic. These levels of overpressuring are indicated by work carried out by Gratier *et al.* (2002, 2003), who showed that fluid pressures in coastal faults in southern California may approach lithostatic pressures at shallow levels in the Earth's crust due to a combination of the mechanisms cited above. Boundary conditions along the bottom margin of the grid were no fluid flow and a constant heat flow of 85 mW m^{-2} (Henyey 1976). An isotherm boundary condition of 20°C was assumed across the subaerial portion of the top margin of the grid. For the submarine portion, an isotherm boundary condition of 13°C was assigned, consistent with observed mid-latitude ocean temperatures to depths of a few hundred meters (Knauss 1996). Exceptions to these boundary conditions occurred where the top grid margin was intersected by the Refugio-Carneros and Coast faults. Here zero heat flow was prescribed to emulate a sea floor spring discharge condition and to prevent temperature increases caused by rapid upward groundwater advection in the faults from being suppressed by an imposed isotherm. Hydraulic head along the top boundary was set equal to topographic elevation from the Refugio-Carneros fault northward, and to be equal to sea level from the Refugio-Carneros fault southward. The vertical boundaries of the grid were assumed to be no-flow boundaries for both fluid and heat.

Three simplified groundwater compositions were included in the models and are described in Table 2. The list of aqueous and mineral phases considered is shown in Table 3. The resident basinal fluid was assumed to be

Table 2 Concentrations (mol l^{-1}) of geochemical components used in reactive transport simulations.

Component	Meteoric recharge	Methane-rich basinal fluid	Methane-poor basinal fluid
Na^+	1.3×10^{-4}	4.8×10^{-1}	4.8×10^{-1}
Ca^{2+}	1.0×10^{-4}	1.0×10^{-2}	1.0×10^{-2}
Cl^-	1.3×10^{-4}	5.0×10^{-1}	5.0×10^{-1}
HS^-	1.0×10^{-7}	1.0×10^{-4}	1.0×10^{-4}
SO_4^{2-}	1.0×10^{-3}	1.0×10^{-7}	1.0×10^{-7}
CH_4^0	1.0×10^{-5}	5.0×10^{-2}	1.0×10^{-5}
SiO_2^0	1.1×10^{-4}	2.5×10^{-4}	2.5×10^{-4}
pH	8.5	7.5	7.0

Table 3 List of aqueous species (components and secondary) and mineral phases considered in the modeling.

Component	Secondary aqueous species		Minerals	
H_2O	Species	Formation reaction	Species	Formation reaction
OH^-	H^+	$H+ = H_2O–OH^-$	Calcite	$CaCO_3 = CH_4^0 + SO_4^{2-} + Ca^{2+} + OH^- - HS^- - 2H_2O$
Na^+	HCO_3^-	$HCO_3^- = CH_4^0 + SO_4^{2-} - HS^- - H_2O$	Quartz	$SiO_2 = SiO_2^0$
Ca^{2+}	CO_3^{2-}	$CO_3^{2-} = CH_4^0 + SO_4^{2-} + OH^- - HS^- - 2H_2O$		
Cl^-	H_2S^0	$H_2S^0 = HS^- + H_2O–OH^-$		
HS^-	$NaCl^0$	$NaCl^0 = Na^+ + Cl^-$		
SO_4^{2-}	$CaCl^+$	$CaCl^+ = Ca^{2+} + Cl^-$		
CH_4^0	$CaCl_2^0$	$CaCl_2^0 = Ca^{2+} + 2Cl^-$		
SiO_2^0	CO_2^0	$CO_2^0 = CH_4^0 + SO_4^{2-} - HS^- - OH^- - H_2O$		

Equilibrium between components SO_4^{2-} and HS^-, which are not linearly independent, was used to define redox state in the simulations.

reducing, slightly alkaline, and to have a salinity similar to that of modern-day seawater, based on fluid inclusion bulk salinity data and well head samples (Boles *et al.* 2004; J.R. Boles, unpublished data). The main objectives of the solute transport calculations were to model the transport and oxidation of methane to form calcite. Thus, numerous chemical species known to be abundant in seawater but not directly pertinent to the transport of methane or precipitation of calcite were omitted from the model to simplify the calculations.

Significant reservoirs of methane occur across much of the stratigraphic section in the Santa Barbara Basin. Likely source formations of methane are limited to a smaller portion of the stratigraphy. The most important source of methane in the basin appears to be the Miocene Monterey Formation, with lesser amounts possibly sourced from the Pliocene Repetto Formation, the Miocene Rincon Shale, and the Eocene Anita Formation and Cozy Dell Shale (Nagle & Parker 1971; Galloway 1998; Tennyson & Isaacs 2001). The Monterey and Repetto formations are stratigraphically and structurally above the calcite cementation in the Refugio-Carneros fault. To result in fault cementation, methane derived from these formations would had to have migrated down section which, although conceivable, has not been implemented in this numerical model. The Rincon Shale intersects the Refugio-Carneros fault near the site of calcite mineralization and could conceivably have been a source of methane if the portion near the fault had been buried more deeply in the past than it is now. The present study examines a scenario in which methane is transported along the Refugio-Carneros fault from depth, consistent with the fluid inclusion homogenization temperature data in the calcite fault cements that indicate rapid fluid fluxes along the fault from depth. Thus in the models, the lowest shale unit in the Paleogene section, which would correspond to the Anita Shale, was assigned an initially high methane concentration of 0.05 mol l^{-1}, a value that reflects the solubility of methane in a moderately saline fluid at temperatures below 250°C and pressures on the order of 10^2 bars (Hanor 1980). In addition, those portions of the Monterey Formation, Rincon Shale, and the undifferentiated Late Miocene-Pleistocene sediments that lie at depths greater than about 1 km and are more favorable for methanogenesis, i.e., the portions south of the Coast fault, were also assigned initially high methane concentrations of 0.05 mol l^{-1}. Elsewhere in the basin, the resident fluid was assigned a low methane concentration of 10^{-5} mol l^{-1} but otherwise had the same composition as the methane-rich fluid. The third fluid considered in the model was a dilute, oxidizing, meteoric fluid that entered the basin along a row of constant source nodes extending along the top margin of the grid from the northern terminus to its intersection with the Refugio fault, an interval corresponding to the subaerially exposed portion of the basin that would have been subject to meteoric recharge.

In summary, the geologic scenario modeled represents a time shortly after the uplift of the Santa Ynez Mountains when meteoric water began to infiltrate the Santa Barbara Basin on a large scale. Methanogenesis in the source formations noted above had already progressed to the point that the formation water there was saturated with respect to methane. The rate of meteoric water infiltration is assumed to have been fast relative to the rate of methane generation, so that no further methane generation occurred during the model simulations beyond what was initially present at the start of the simulations after uplift, thus effectively only making one pore volume of methane-rich fluid in the formation available for reaction. Ongoing north–south-directed tectonic shortening of the basin led to episodic overpressure development and fluid expulsion in the Refugio-Carneros and Coast fault zones because of compaction and sealing of fault gouge and its subsequent rupture. Methane-rich fluids that intersected these faults were transported to higher stratigraphic levels where they were able to mix with infiltrating meteoric fluids, causing methane to become oxidized to carbonate, and leading to the precipitation of calcite. High fluid flow rates in the faults also led to significant transport of heat, causing the elevated fluid temperatures recorded by fluid inclusions in the calcite fault cement.

HYDROLOGIC MODELING RESULTS

Figure 5 illustrates the evolution of the hydraulic head in the basin for the base case scenario described in Table 1 immediately after fault rupture. Hydraulic head is represented by a relative overpressuring term, λ^*, defined as $(h - h_H)/(h_L - h_H)$, where h is the hydraulic head, h_H is hydrostatic head, and h_L is lithostatic head. From this relationship it is evident that λ^* will have a positive value when the hydraulic head is greater than hydrostatic (i.e., overpressured), reaching a maximum value of 1 when the hydraulic head is equal to lithostatic head. Further, λ^* will have a value of zero when hydraulic head is equal to hydrostatic head and a negative value when hydraulic head is lower than hydrostatic head (i.e., underpressured). As noted previously, hydraulic heads were assumed to be initially hydrostatic throughout the basin except in the Refugio-Carneros and Coast faults, where they were assumed to be overpressured to up to 80% of lithostatic. Overpressures diffuse rapidly out of the faults, decaying to a third of their initial value or less over much of the fault length within 10 years. Diffusion of overpressures is most rapid over the middle portions of the faults, where the hydrogeologic units intersecting the faults have both low matrix compressibility and high hydraulic conductivity. By 100 years, overpressures in the faults have dissipated to essentially background hydrostatic levels.

Because of the large, order-of-magnitude variations in fluid velocity predicted in the simulations, fluid flow patterns are best represented by the stream function shown in Fig. 6. The results plotted are for a time of 200 years, when overpressures in the faults have largely diffused into the surroundings and the system is approaching a hydrologic steady-state. Because the mass fluid flux is equivalent between any two streamlines, the more closely packed the streamlines are over an area the greater the groundwater flow velocities. Slight changes to the flow patterns depicted in Fig. 6 occur at early times in the immediate vicinity of the faults, where high initial heads can temporarily drive fluid away from the faults. At late times, flow in the faults reverses direction and is downward instead of upward. Little fluid flow occurs in the low permeability Jalama Formation in the northernmost and lower part of the grid. South of the topographic maximum and corresponding hydraulic divide, fluid moves more rapidly down the steeply dipping Cenozoic sediments, particularly the more permeable sandstone units. Some fluid in the steeply dipping sediments is entrained by the Refugio-Carneros fault while most of the remainder continues southward, though generally at a lower velocity because of the constant head boundary condition at the top margin of the grid south of the fault created by the presence of the sea. Most of the remaining fluid is entrained by the Coast fault, though fluid velocities are slightly lower there than in the Refugio-Carneros fault.

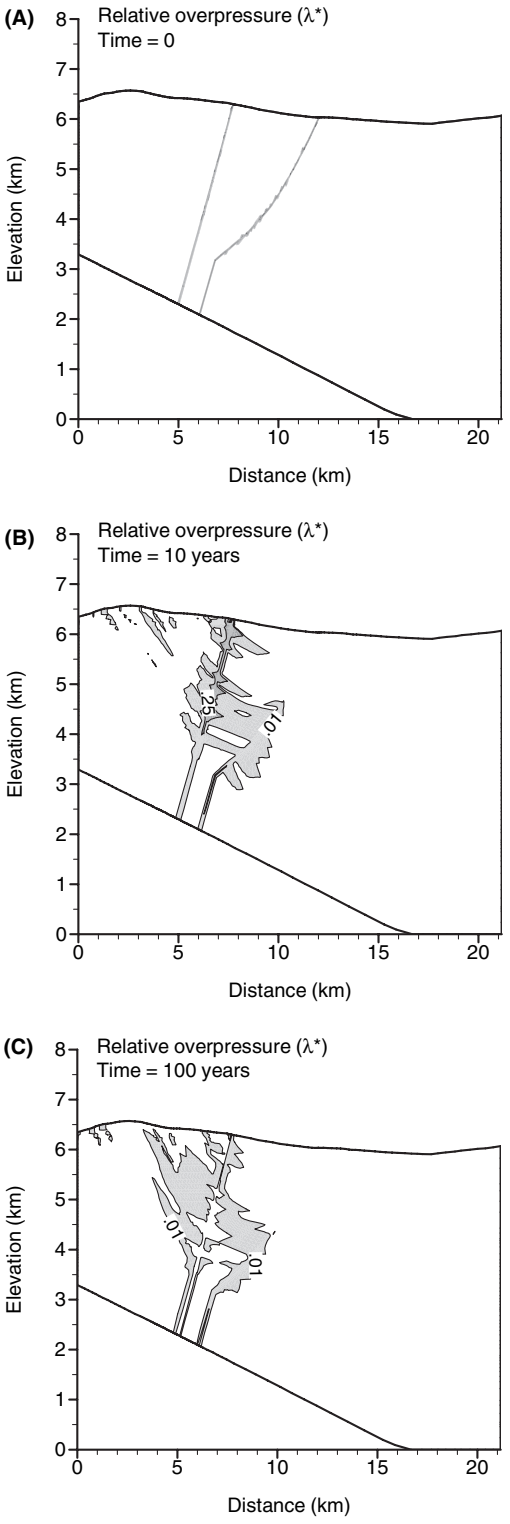

Fig. 5. Evolution of relative overpressuring in the Santa Barbara Basin over time following fault rupture at (A) time = 0, (B) time = 10 years, (C) time = 100 years. The relative overpressuring is expressed as $\lambda^* = (h - h_H)/(h_L - h_H)$, where h is the hydraulic head, h_H is hydrostatic head, and h_L is lithostatic head.

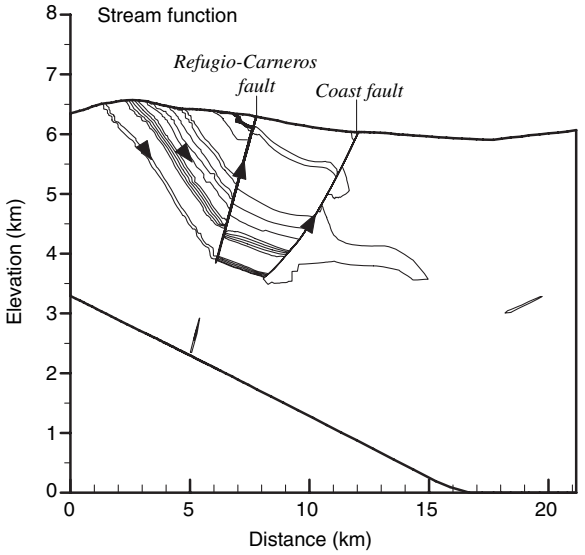

Fig. 6. Stream function after 200 years of simulation time, showing fluid flow patterns in the basin. The contour interval is 2976 kg m^{-1} $year^{-1}$. Higher densities of streamlines indicated higher fluxes of fluid flow. Thus, the highest fluxes occur in the Vaqueros Sandstone (cf. Figs 3 and 4). The results show fluids entering the basin in the topographically high northern margin of the basin in the Santa Ynez Mountains and descending the steeply dipping strata occurring there. Much of the fluid is captured by the Refugio-Carneros and Coast faults and rises to the surface. Flow rates diminish south of the Coast fault where the hydraulic head gradient diminishes.

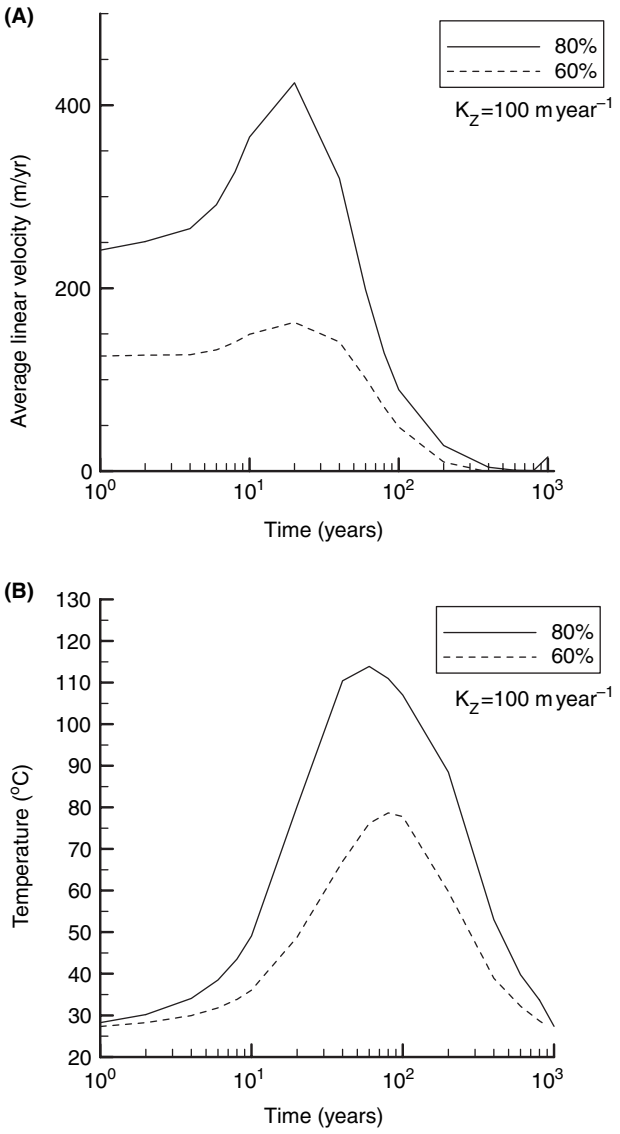

Fig. 7. Evolution after fault rupture of (A) average linear groundwater velocity and (B) temperature (°C) over time in the top 200 m of the Refugio-Carneros fault for a vertical fault hydraulic conductivity of 100 m $year^{-1}$ and initial overpressures of 60% and 80% of lithostatic.

This greater degree of fluid capture is due in large part to the greater amount of stratigraphic displacement on the Coast fault compared to the Refugio-Carneros (Fig. 6), rather than to a difference in hydraulic conductivities, which are the same for both faults. Among the sedimentary units, the greatest flux of fluid occurs in the Vaqueros Sandstone (cf. Fig. 3), which has a lateral hydraulic conductivity equivalent to that of the faults in the base case simulation. Lateral average linear velocities in the Vaqueros range from several meters per year in the north to several tenths of meters per year in the south. As with the other sedimentary units, some fluid in the Vaqueros is captured by the Refugio-Carneros fault. South of the Coast fault, fluid flow velocities gradually diminish in all of the units as a result of the dampening effects on the hydraulic head gradient caused by the constant head boundary condition equal to sea level along the top grid margin.

The high degree of overpressuring in the faults causes a transient upsurge of fluid within them that builds to a maximum velocity over approximately the first 20 years of the simulation and gradually decays thereafter, approaching a steady-state value after a few hundred years. This behavior is shown in Fig. 7(A) for a point located near the top of the Refugio-Carneros fault, approximately 200 m below the ground surface. Vertical average linear velocities at this point reach a maximum of about 420 m $year^{-1}$ and decay to a value around 1 m $year^{-1}$ by 1000 years. Lowering the degree of overpressuring in the faults from 80% to 60% of lithostatic diminishes fluid velocities. Maximum vertical average linear velocities in the top 200 m of the Refugio-Carneros fault diminish to about 160 m $year^{-1}$ but approach approximately the same steady-state value of around 1 m $year^{-1}$ after 1000 years.

The transient upsurges in fluid flow in the faults create transient increases in temperature (Figs 7B and 8). At a fault overpressure of 80% of lithostatic, temperature in the top 200 m of the Refugio-Carneros fault reaches 114°C after about 60 years, decaying to 30°C by 1000 years, which is near the steady-state value. A decrease in fault overpressure to 60% of lithostatic delays the arrival of the

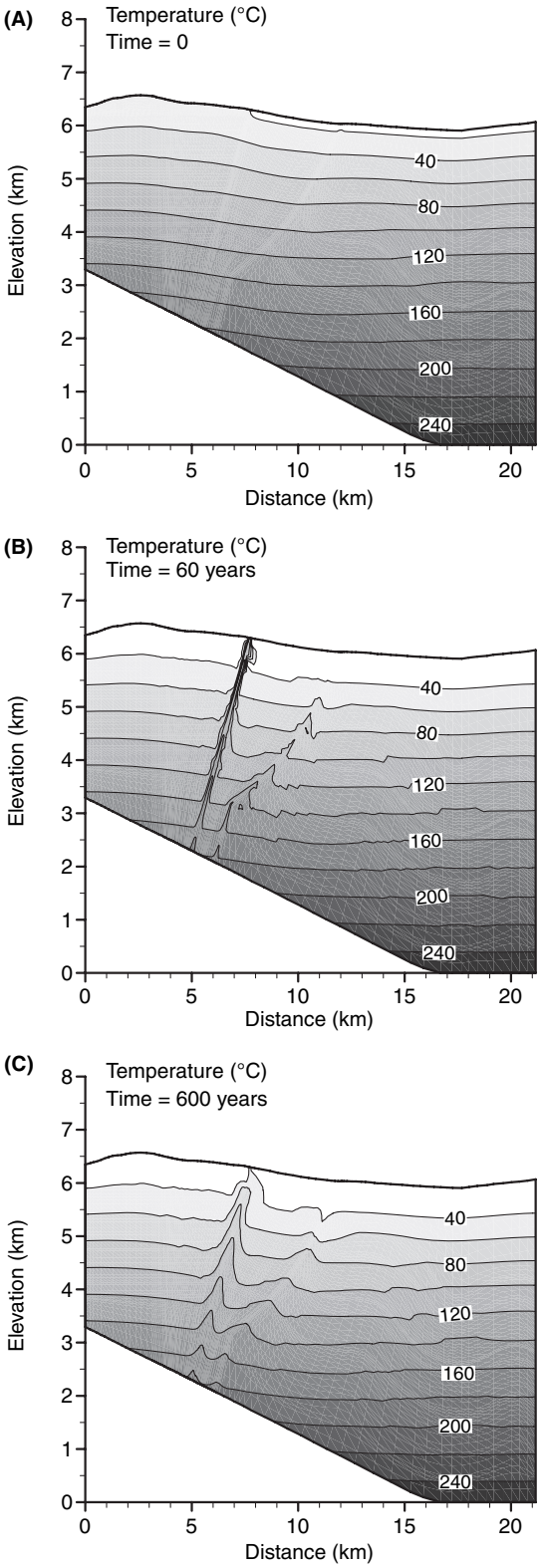

Fig. 8. Temperature (°C) evolution over time following fault rupture shown at (A) time = 0, (B) time = 60 years, and (C) time = 600 years.

temperature maximum to about 74 years and lowers its magnitude to about 78°C. Thus, at a fault hydraulic conductivity of 100 m year^{-1}, overpressures >60% of lithostatic and approaching 80% or greater are needed to generate the temperatures indicated by fluid inclusions in the calcite fault cements.

Figure 9 also displays average linear velocity and temperature as a function of time in the upper 200 m of the Refugio-Carneros fault and illustrates the effect of raising the fault hydraulic conductivities from 100 to 500 m year^{-1}. The higher hydraulic conductivity leads to a more rapid diffusion of overpressures out of the fault, and to a corresponding earlier arrival in the temperature maxima by about a factor of 5 over the lower hydraulic conductivity case. As in the lower hydraulic conductivity case,

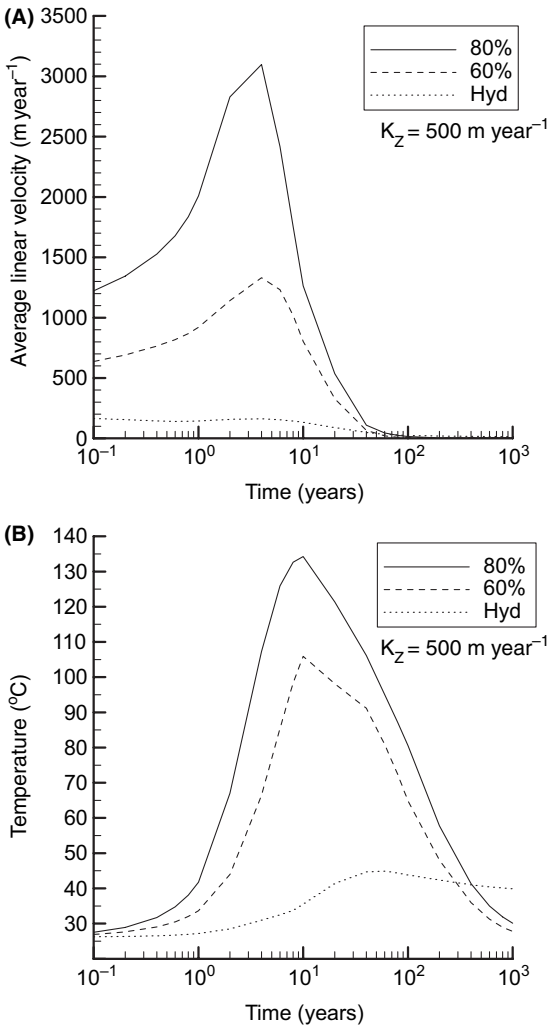

Fig. 9. Evolution after fault rupture of (A) average linear groundwater velocity and (B) temperature (°C) over time in the top 200 m of the Refugio-Carneros Fault for a vertical fault hydraulic conductivity of 500 m year^{-1} and initial hydraulic heads of hydrostatic and 60% and 80% of lithostatic.

the average linear velocity maximum precedes the temperature maximum, but the magnitudes of velocity and temperature are both significantly greater in the higher hydraulic conductivity case. Maximum velocities reach about 3100 and 1300 m year^{-1} after about 4 years and maximum temperatures reach about 134 and 106°C after about 10 years at overpressures of 80% and 60% of lithostatic head, respectively. The results show that higher fault hydraulic conductivity promotes greater heat transport, allowing a lower degree of overpressuring to account for the temperatures recorded by the fluid inclusions in the fault cements. However, near-hydrostatic pressures could not generate the necessary heat transport, even at fault hydraulic conductivity values significantly higher than for the 500 m year^{-1} case shown in Fig. 9. This indicates that a topography-driven flow system is unlikely to have been sufficient to account for the observed fluid inclusion temperatures and that some mechanism of overpressuring was probably needed.

REACTIVE TRANSPORT SIMULATIONS

As described above, the purpose of the reactive transport simulations was to test the effects of mixing of oxidizing meteoric water entering the basin as recharge in the Santa Ynez Mountains with more saline methane-rich basinal fluids. In the models, these methane-rich basin fluids were restricted to potential shale source rocks near the base of the Paleogene sedimentary sequence, corresponding approximately to the Anita Shale, and to the Monterey Formation and Rincon Shale at depths greater than about 1 km from the surface (Fig. 3). The remainder of the basin was assumed initially to contain a saline fluid of similar composition but a low methane content of 10^{-5} mol l^{-1} instead of 0.05 mol l^{-1}. Meteoric recharge was allowed to enter the basin along a row of constant source nodes extending along the top margin of the grid from the northernmost boundary to the Refugio-Carneros fault, beyond which the basin was considered to be submarine. The Refugio-Carneros and Coast faults were not initially overpressured in the reactive transport simulations, but were initially assigned hydrostatic head values and low hydraulic conductivities to represent a period of fault sealing.

Figure 10 shows the concentration of total chloride (i.e., the sum of all chloride species in solution) after 30 000 and 75 000 years. Fresh water can be seen to migrate preferentially through the permeable sandstone units of the Paleogene sedimentary package and through the Vaqueros Sandstone. Fresh water migrating through the Vaqueros Sandstone reaches the Refugio-Carneros fault in only a few hundred years. However, the low permeability of the fault greatly hinders movement of fresh water past the fault and causes the fresh water primarily to be deflected upward parallel to it. Once the fresh water plume from the Vaqueros

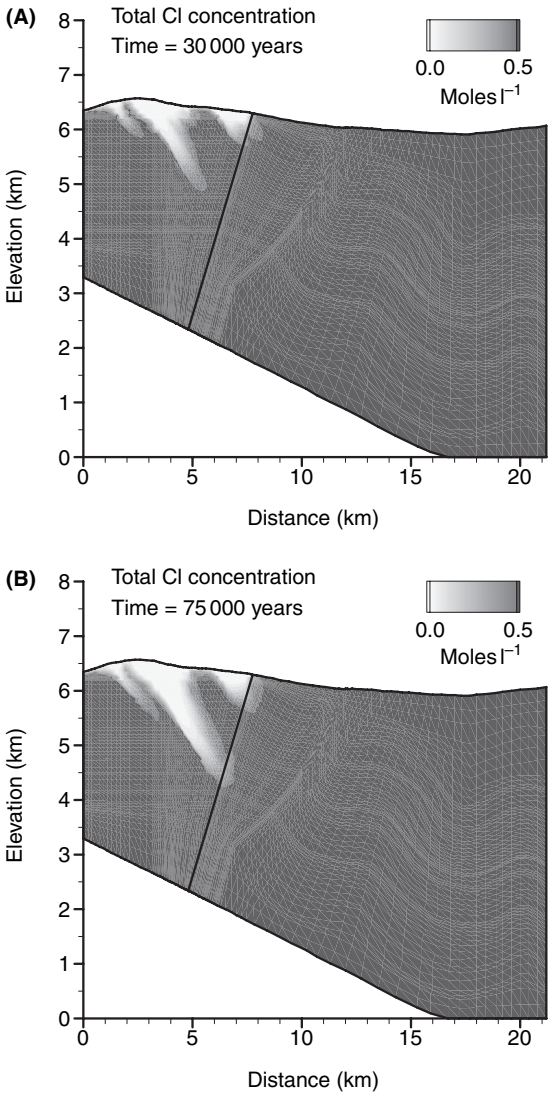

Fig. 10. Total chloride concentration (sum of all chloride species) as a function of time at (A) 30 000 years and (B) 75 000 years of simulation time, showing the advance of fresh meteoric water plumes from the recharge area in the Santa Ynez Mountains.

Sandstone has reached the Refugio-Carneros fault, it provides a means to oxidize any methane rising along the fault from depth in the basin. Eventually, fresh water plumes in other hydrostratigraphic units fed by meteoric recharge at the surface also reach the Refugio-Carneros fault, allowing for potential oxidation of methane deeper in the basin.

A further important result of the simulations is that even after the fresh water plumes traveling through the more permeable hydrostratigraphic units have reached the Refugio-Carneros fault, no calcite mineralization develops in the fault until there is a release of overpressured fluids from the methane source region. This is because the topographically generated hydraulic head gradient is too low to drive methane-rich fluid from the base of the Paleogene section

up the fault to supply the carbon needed for calcite precipitation. In addition, methane-rich fluids south of the Refugio-Carneros fault would have little means of reaching the fault in the absence of another fluid flow mechanism because the prevailing direction of groundwater flow based on the topographic gradient is from north to south. Thus, the development of overpressure in the Refugio-Carneros fault after the time that meteoric water had reached the fault from recharge areas in the Santa Ynez Mountains was necessary in the models to produce calcite mineralization in the fault.

The first of these renewed overpressures of 80% of lithostatic was inserted into the models at 10 000 years at which time the fault was also made open to fluid flow (Table 1), and this sequence was repeated thereafter at 1000 year intervals. Figure 11 shows the ascent of methane-enriched plumes of basinal fluid along the Refugio-Carneros and Coast faults at 10 002 and 10 008 years. The results show that methane-rich fluids with concentrations on the order of about 10^{-3} mol l^{-1} have reached the upper 200 m of the Refugio-Carneros fault within only a few years. Methane-rich fluids continue to ascend the faults for the remainder of the 1000 year interval, though at progressively slower rates (cf. Fig. 7A). This ascent now allows the precipitation of calcite to begin as oxidizing meteoric water and methane-rich fluids have now been brought into contact with one another.

The distribution of calcite precipitation after 10 100 and 11 000 years is shown in Fig. 12 for a portion of the basin centered on the top of the Refugio-Carneros fault. The figure shows the effects of a single pulse of methane-rich basinal fluid mixing over a 1000-year period with a fresh water plume already in place in the upper aquifers (cf. Fig. 10). Weak calcite mineralization on the order of 10^{-1} mol m^{-3} BPM develops in the Vaqueros Sandstone a few hundred meters north of its intersection with the Refugio-Carneros fault. (Note that in computing this mol m^{-3} BPM concentration, it is assumed that the length in the third dimension, i.e., perpendicular to the plane of the cross section, is 1 m.) The mineralization initially develops north of the fault in part because fresh water invasion has progressed further on the north side of the fault than on the south side. In addition, as high hydraulic heads in the fault at the time of rupture begin to diffuse outward, fluid moves away from the fault in response to the head gradient produced. Methane-rich fluids that had been ascending the fault then begin displacing the descending meteoric water, creating a mixing zone, and hence calcite precipitation zone, slightly offset from the fault to the north. With increasing time, the overpressure-induced hydraulic head gradient around the Refugio-Carneros fault weakens and the hydraulic head pattern returns to a topography-driven one in which head decreases from north to south. As fluid north of the fault begins to flow south again, the mixing zone between oxidizing meteoric water and methane-rich fluid shifts southward and becomes centered on the fault, where the greatest quantities of calcite are also precipitated. Lesser quantities of calcite are precipitated in the Vaqueros Sandstone south of the Refugio-Carneros fault, as the meteoric water plume descending the Vaqueros entrains methane as it passes the fault.

The greatest concentration of calcite mineralization occurs in the upper several hundred meters of the Refugio-Carneros fault (Fig. 12B). After 11 000 years, which

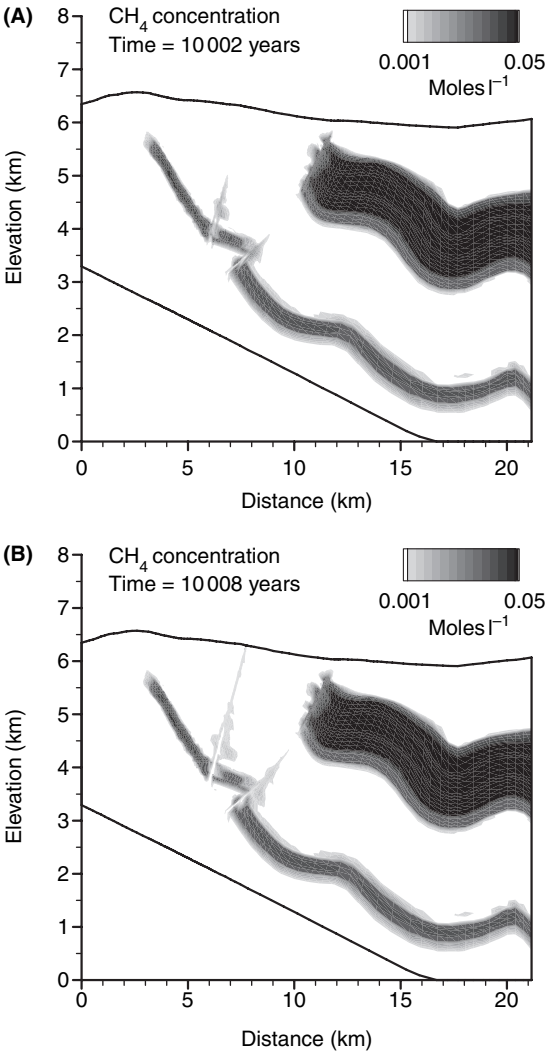

Fig. 11. Methane concentration at (A) 10 002 years and (B) 10 008 years. Methane-rich (0.05 mol l^{-1}) pore fluids were initially assigned to portions of the Anita Shale, Monterey Formation, Rincon Shale, and Miocene–Pleistocene sediments that lay at depths of greater than about 1 km in the model cross section. The simulation was first run to 10 000 years to allow thorough invasion of the fresh meteoric water plume in the Vaqueros Sandstone as far as the Refugio-Carneros fault. At 10 000 years, overpressures of 80% of lithostatic were assigned to the Refugio-Carneros and Coast faults. Continuation of the simulation beyond 10 000 years showed methane-rich fluid being transported up the faults from the Anita Shale.

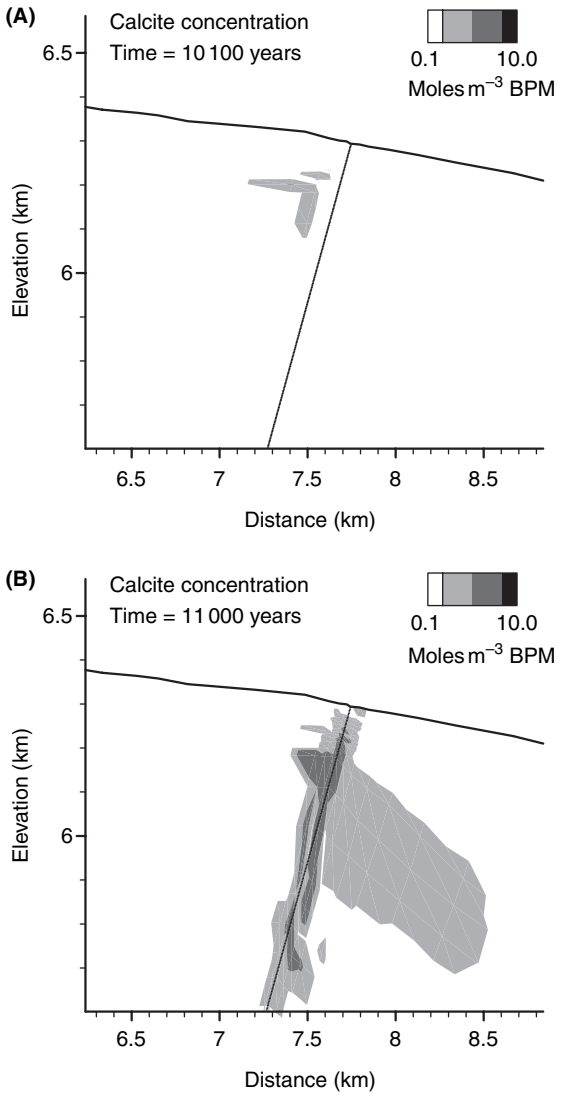

Fig. 12. Calcite mineralization at (A) 10 100 years and (B) 11 000 years shown for a region centered on the upper 200 m of the Refugio-Carneros fault (cf. Fig. 3). The mineralization is produced in a mixing zone within the fault itself and immediately adjacent to the fault on its north side. All of the mineralization is produced from the methane transported from a single pulse of fluid initiated by the emplacement of overpressuring along the fault at 80% of lithostatic at 10 000 years. Within 1000 years after fault rupture, upward fluid flow, and hence upward solute flux, has largely subsided (cf. Fig. 7A) and little additional accumulation of calcite mineralization occurs.

represents the end of the first fault overpressuring event and the time immediately prior to the onset of the next one, calcite concentrations have reached a maximum of nearly 7 mol m^{-3} BPM within the fault. If the volume over which calcite mineralization occurred in the model at this concentration equaled the $1.5 \times 15 \times 15$ m volume of calcite occurring in the corresponding field location (Boles *et al.* 2004), a plausible scenario given that the areal distribution of mineralization in the model exceeds the areal distribution in the field, then about 3800 such fault pulses would be required to produce the entire mass of calcite observed in the field. If the fault pulses occurred at 1000 year intervals as in the models, then about 3.8 Myr would be needed to form the calcite. The time required for calcite mineralization could be reduced if the fault pulse interval were shorter, the fault permeability were higher, methane concentrations were higher, perhaps even to the point where some methane was transported as a separate fluid phase, or if higher hydraulic diffusivities existed in the country rocks.

If the cross-sectional area through which fluid in the Refugio-Carneros fault flows is the 10 m minimum width of the fault zone multiplied by the 15 m length of the mineralization, and if the effective porosity of the fault zone is 10%, then integrating over the first 100 years of the 80% of lithostatic average linear velocity curve in Fig. 7A, which is when the flow and methane concentrations are the highest, would lead a volume of fluid for each fault pulse of about 3.5×10^5 m^3. If the fluid ascending the fault were able to maintain a methane concentration of 0.01 mol l^{-1} (slightly lower than the concentration prescribed to the source area), then only about three fault pulses would be required to produce all of the observed calcite in the Refugio-Carneros fault. The models however predict the calcite mineralization process to be considerably less efficient than this. In part this is caused by dispersion, which causes the concentration of the methane arriving at the mineralization site to be diminished well below the level at the source. In addition, the methane-rich basinal fluid tends to displace the oxidizing meteoric fluid rather than to become entrained within it, causing only the fringes of the solute plumes in the two fluids to interact with one another and thus leaving much of the methane unoxidized.

DISCUSSION

The results of this study indicate conditions under which calcite in the Refugio-Carneros fault could have formed by mixing of meteoric water descending from the Santa Ynez Mountains on the northern flank of the basin with rising methane-rich basinal fluids driven by fault overpressures. The modeling shows that meteoric fluids would have been capable of descending the steeply dipping sediments on the northern flank of the basin, and where the hydraulic conductivities were high, such as in the Vaqueros Sandstone, could have reached the Refugio-Carneros fault in a relatively short period of time. Though any of the sandstone units cropping out at the northern end of the basin could have transmitted significant fluxes of meteoric fluid, the Vaqueros is a particularly important conduit because it is at its intersection with the Refugio-Carneros fault that the calcite cements are found. Methane in quantities sufficient

to account for the observed amount of calcite cement in the fault could conceivably have been derived from one of several possible stratigraphic units in the basin (Nagle & Parker 1971; Galloway 1998), though most of the hydrocarbons in the basin appear to have been derived from the Monterey Formation (Curran *et al.* 1971; Isaacs & Petersen 1987; Keller 1990). The scenario modeled in which the Eocene Anita Shale, the Late Miocene-Pleistocene sediments, and the deeper portions of the Monterey Formation and Rincon Shale south of the Coast fault were the principal methane sources represents one of the more difficult scenarios to realize in that most of the methane contributing to calcite precipitation in the fault was derived from the Anita Shale and traversed one of the longer possible vertical transport distances in the basin. The fact that calcite was easily precipitated under this scenario means that calcite would have been formed with even less difficulty if the methane had been derived from a shallower source that intersected the Refugio-Carneros fault. The calcite formation process however was not very efficient in the models, requiring about 3800 fault pulses to account for the entire mass of calcite observed in the field. Thus, at a fault pulse interval of 1000 years as used in the models, approximately 3.8 Myr would be required to form the calcite. This period is probably too long, as the meteoric flow regime that would have oxidized the methane probably did not exist until the beginning of deposition of the coarse clastic Santa Barbara Formation, which is believed to be no older than about 1 Ma (Huftile & Yeats 1995). The time needed for calcite deposition could be shortened if the fault pulse interval were shorter, but the high number of fault pulses required may also be problematic as no clear evidence for this has been recognized in the field, e.g., in the form of discrete brecciation events. The models thus may point to the need for a more efficient mixing mechanism between the basinal and meteoric fluids, perhaps through the inducement of turbulence in the mixing zone, or for a more continuous or concentrated source of methane.

Though fault overpressuring was not found to be an efficient means of solute transport in the models, it was found to be an effective means for vertical heat transport and raising the temperature in the upper 200 m of the fault to the approximately 100°C values indicated by the fluid inclusion data. Without fault overpressuring, the remaining driving force for fluid flow was the gradient in elevation of the water table and this was insufficient to produce the upward fluxes of heat needed to account for the observed temperatures. In fact, at longer times of thousands to tens of thousands of years as the flow system approaches a steady-state dominated by topography-driven flow, fluid flow in the Refugio-Carneros fault becomes directed downward preventing temperature elevation.

The models did not incorporate an explicit mechanism for overpressure generation. However, based on previous work by Byerlee (1990, 1993), Rice (1992), Sleep & Blanpied (1992), and Gratier *et al.* (2002, 2003), much of it specifically in reference to geologically young faults in southern California, overpressures could plausibly have been produced in the Refugio-Carneros and Coast faults at levels approaching lithostatic due to a combination of crack sealing by pressure solution and fault gouge compaction during fault compression, and fluid flow from higher pressure environments at depth. These overpressures would have been largely confined to the faults until earthquakes increased their porosity and permeability, allowing the overpressures to diffuse into the surrounding rocks. Thus the faults would have experienced histories of episodic overpressure build-up and release on time scales probably on the order of thousands of years, though shorter intervals are possible. This was modeled in the present study simply by assigning instantaneous overpressures in the faults at prescribed times and allowing the overpressures to begin diffusing away immediately thereafter.

Other mechanisms for overpressuring could possibly have existed in the Santa Barbara Basin during the time of calcite mineralization in the Refugio-Carneros fault. The active hydrocarbon generation that has occurred during much of the basin's history suggests the possibility of overpressures developing at depth through methanogenesis. Alternatively, the rapid deposition, relatively young age, and low permeability of much of the sediment suggest that disequilibrium compaction may have been occurring in the basin and led to the development of overpressures. Both mechanisms could potentially have provided a long-lived driving force for fluid flow up the faults and laterally from the southern part of the basin, at the same time providing the means for heat and solute transport. Investigation of these mechanisms was outside of the scope of the present study, but is suggested as a possibility for future work.

CONCLUSIONS

Numerical reactive transport modeling has demonstrated conditions under which massive calcite cement in the Refugio-Carneros fault could have precipitated by mixing of oxidizing meteoric water driven by topography with methane-rich basinal fluid driven by fault overpressuring. The results show that meteoric fluid could have entered the Santa Barbara Basin as recharge in the Santa Ynez Mountains and flowed through the Vaqueros Sandstone to its intersection with the Refugio-Carneros fault and beyond. Methane-rich basinal fluids could have risen along the faults from deeper source regions in the basin provided the faults were episodically overpressured and episodically permeable. Overpressuring and high permeability in the faults were also needed to allow the amount of heat

transport necessary to raise temperatures in the upper 200 m of the Refugio-Carneros fault to the 80–125°C range indicated by fluid inclusions in the calcite. If methane concentrations in the source formations were near the saturation level expected at kilometer-scale depths, fault hydraulic conductivity was on the order of at least 100 m $year^{-1}$, maximum overpressure in the faults before rupture was around 80% of lithostatic or more, and the frequency of fault rupture was around 1000 years, then the mass of calcite found in the Refugio-Carneros fault could be produced in a few million years or less by the scenario modeled. However, the length of time and number of fault pulses needed to produce the calcite mineralization were probably difficult to attain given the tectonic and sedimentary environment in the recent history of the basin, and point to the need to explore alternate mechanisms for solute transport.

ACKNOWLEDGMENTS

Funding for this research was provided from grants DE-FG02-96ER14619 and DE-FG02-96ER14620 from the U.S. Department of Energy, Office of Basic Energy Sciences. The authors would also like to acknowledge the reviews of two anonymous *Geofluids* referees whose contributions significantly improved the manuscript.

REFERENCES

Blackwell DD, Steele JL (1989) Thermal conductivity of sedimentary rocks: measurement and significance. In: *Thermal History of Sedimentary Basins: Methods and Case Histories* (eds Naeser ND, McCulloh TH), pp. 13–36. Springer-Verlag, New York.

Boles JR, Grivetti M (2000) Calcite cementation along the Refugio/Carneros fault, coastal California: a link between deformation, fluid movement and fluid-rock interaction at a basin margin. *Journal of Geochemical Exploration*, **69–70**, 313–316.

Boles JR, Clark JF, Leifer I, Washburn L (2001) Temporal variation in natural methane seep rate due to tides, Coal Oil Point area, California. *Journal of Geophysical Research*, **106C**, 27077–27086.

Boles JR, Eichhubl P, Garven G, Chen J (2004) Evolution of a hydrocarbon migration pathway along basin-bounding faults: evidence from fault cement. *American Association of Petroleum Geologists Bulletin*, **88**, 947–970.

Briggs RW (2003) Revised waste discharge requirements for Tajiguas class III landfill, Santa Barbara County. *California Regional Water Quality Control Board*, Draft WDR R3-2003-0011, 1–19.

Byerlee J (1990) Friction, overpressure and fault normal compression. *Geophysical Research Letters*, **17**, 2109–2112.

Byerlee J (1993) Model for episodic flow of high-pressure water in fault zones before earthquakes. *Geology*, **21**, 303–306.

Crouch JK (1979) Neogene tectonic evolution of the California Continental Borderland and western Transverse Ranges. *Geological Society of America Bulletin, Part I*, **90**, 338–345.

Curran JF, Hall KB, Herron RF (1971) Geology, oil fields, and future petroleum potential of Santa Barbara channel area, California. In: *Future Petroleum Provinces of the United States – Their Geology and Potential*, Memoir 15 (ed. Cram IH), pp. 192–211. American Association of Petroleum Geologists, Tulsa, OK.

Eichhubl P, Behl RJ (1998) Field guide to 'Diagenesis, deformation, and fluid flow in the Miocene Monterey Formation': Ventura—Santa Barbara—Jalama Beach—Grefco Quarry/Lompoc. In: *Diagenesis, Deformation, and Fluid Flow in the Miocene Monterey Formation*, Pacific Section SEPM Special Publication Book 83 (ed. Eichhubl P), pp. 85–98. SEPM, Los Angeles, CA.

Eichhubl P, Boles J (2000a) Focused fluid flow along faults in the Monterey formation, coastal California. *Geological Society of America Bulletin*, **112**, 1667–1679.

Eichhubl P, Boles J (2000b) Rates of fluid flow in fault systems – evidence for episodic rapid fluid flow in the Miocene Monterey formation, coastal California. *American Journal of Science*, **300**, 571–600.

Eichhubl P, Greene HG, Naehr T, Maher N (2000) Structural control of fluid flow: offshore fluid seepage in the Santa Barbara basin, California. *Journal of Geochemical Exploration*, **69–70**, 545–549.

Freeze RA, Cherry JA (1979) *Groundwater*. Prentice-Hall, Upper Saddle River, NJ.

Giallonardo T, Koller A (1978) *Gaviota Offshore Gas Field*. California Department of Conservation, Division of Oil and Gas, Publication No. TR21, Sacramento, CA, 11 pp.

Galloway JM (1998) Santa Barbara-Ventura basin province. In: *Structure and Petroleum Geology, Santa Barbara Channel, California*, Miscellaneous Publication 46 (eds Kunitomi DS, Hopps TE, Galloway JM), pp. 63–72. Pacific Section, American Association of Petroleum Geologists, Bakersfield, CA.

Gelhar LW, Welty C, Rehfeldt KR (1992) A critical review of data on field-scale dispersion in aquifers. *Water Resources Research*, **28**, 1955–1974.

Gorsline DS, Teng LS-Y (1989) The California Continental Borderland. In: *The Eastern Pacific Ocean and Hawaii* (eds Winterer EL, Hussong DM, Decker RW), pp. 471–487. Geological Society of America, Boulder, CO.

Gratier JP, Favreau P, Renard F, Pili E (2002) Fluid pressure evolution during the earthquake cycle controlled by fluid flow and pressure solution crack sealing. *Earth Planets Space*, **54**, 1139–1146.

Gratier JP, Favreau P, Renard F (2003) Modeling fluid transfer along California faults when integrating pressure solution crack sealing and compaction processes. *Journal of Geophysical Research*, **108**, 1–25.

Hanor JS (1980) Dissolved methane in sedimentary brines: potential effect on the PVT properties of fluid inclusions. *Economic Geology*, **75**, 603–617.

Helgeson HC (1969) Thermodynamics of hydrothermal systems at elevated temperatures and pressures. *American Journal of Science*, **267**, 729–804.

Henyey TL (1976) Heat flow and tectonic patterns on the southern California borderland. In: *Aspects of the Geological History of the California Continental Borderland*, Miscellaneous Publication 24 (ed. Howell DG), pp. 427–448. Pacific Section American Association of Petroleum Geologists, Bakersfield, CA.

Hinman NW, Schwartz DE (1990) Lithologic and diagenetic sequences of the Monterey Formation, Molino Field, Offshore Santa Barbara, California. In: *Miocene and Oligocene Petroleum Reservoirs of the Santa Maria and Santa Barbara-Ventura Basins, California: A Core Workshop* (eds Keller MA, McGowen MK), pp. 271–336. SEPM Core Workshop No. 14, Tulsa, OK.

Hornafius JS, Luyendyk BP, Terres RR, Kammerling MJ (1986) Timing and extent of Neogene tectonic rotation in the western

Transverse Ranges, California. *Geological Society of America Bulletin*, **97**, 1476–1487.

Howell DG, Crouch JK, Greene HG, McCulloch DS, Vedder JG (1980) Basin development along the late Mesozoic and Cainozoic California margin: a plate tectonic margin of subduction, oblique subduction and transform tectonics. *Special Publication International Association of Sedimentologists*, **4**, 43–62.

Huftile GJ, Yeats RS (1995) Convergence rates across a displacement transfer zone in the western Tranverse Ranges, Ventura basin, California. *Journal of Geophysical Research*, **100**, 2043–2067.

Isaacs CM, Petersen NF (1987) Petroleum in the Miocene Monterey Formation, California. In: *Siliceous Sedimentary Rock-Hosted Ores and Petroleum* (ed. Hein JR), pp. 83–116. Van Nostrand Reinhold, New York.

Jackson PA, Yeats RS (1982) Structural evolution of Carpinteria basin, western Transverse Ranges, California. *American Association of Petroleum Geologists Bulletin*, **66**, 805–829.

Johnson JW, Oelkers EH, Helgeson HC, 1992, SUPCRT92: a software package for calculating the standard molal thermodynamic properties of minerals, gases, aqueous species, , and reactions from 1 to 5000 bar and 0 to 1000°C. *Computers and Geosciences*, **18**, 899–947.

Keller MA (1990) Introduction to stratigraphy and hydrocarbon occurrence in Oligocene and Miocene rocks of the Santa Barbara-Ventura and Santa Maria basins of California. In: *Miocene and Oligocene Petroleum Reservoirs of the Santa Maria and Santa Barbara-Ventura Basins, California: A Core Workshop* (eds Keller MA, McGowen MK), pp. 1–11. SEPM Core Workshop No. 14, Tulsa, OK.

Keller MA (1995) Ventura basin province (013). In: *National Assessment of United States Oil and Gas Resources – Results, Methodology, and Supporting Data* (eds Gautier D, Dolton GL, Takahashi KI, Varnes KL), U.S. Geological Survey Digital Data Series 30, CD-ROM, Reston, VA.

Knauss JA (1996) *Introduction to Physical Oceanography*. Prentice-Hall, Upper Saddle River, NJ.

Nagle HE, Parker ES (1971) Future oil and gas potential of onshore Ventura basin, California. In: *Future Petroleum Provinces of the United States – Their Geology and Potential* (ed. Cram IH), pp. 254–297. American Association of Petroleum Geologists, Tulsa, OK.

Nicholson C, Sorlien CC, Atwater T, Crowell JC, Luyendyk BP (1994) Microplate capture, rotation of the western Transverse Ranges, and initiation of the San Andreas transform as a low-angle fault system. *Geology*, **22**, 491–495.

Raffensperger JP, Garven G (1995a) The formation of unconformity-type uranium deposits. 1. Coupled groundwater and heat transport modeling. *American Journal of Science*, **295**, 581–630.

Raffensperger JP, Garven G (1995b) The formation of unconformity-type uranium deposits. 2. Coupled hydrochemical modeling. *American Journal of Science*, **295**, 639–696.

Reimers CE, Ruttenberg KC, Canfield DE, Christiansen MB, Martin JB (1996) Porewater pH and authigenic phases formed in the uppermost sediments of the Santa Barbara basin. *Geochimica et Cosmochimica Acta*, **60**, 4037–4057.

Rice JR (1992) Fault stress states, pore pressure distributions, and the weakness of the San Andreas fault. In: *Fault Mechanics and Transport Properties of Rocks* (eds Evans B, Wong T), pp. 475–503. Academic Press, San Diego, CA.

Sabins, FF (1997) *Remote Sensing: Principles and Interpretation*. W. H. Freeman, New York.

Schwartz FW, Zhang H (2003) *Fundamentals of Groundwater*. Wiley & Sons, New York.

Sleep N, Blanpied M (1992) Creep, compaction and weak rheology of major faults. *Nature*, **359**, 687–692.

Tennyson ME, Isaacs CM (2001) Geologic setting and petroleum geology of Santa Maria and Santa Barbara basins, coastal California. In: *The Monterey Formation; From Rocks to Molecules* (eds Isaacs CM, Rullkoetter J), pp. 206–229. Columbia University Press, New York.

Tennyson ME, Kropp AP (1998) Regional cross section across Santa Barbara Channel from northwestern Santa Rosa Island to Canada de Molino. In: *Structure and Petroleum Geology, Santa Barbara Channel, California*, Miscellaneous Publication 46 (eds Kunitomi DS, Hopps TE, Galloway JM), pp. 185–193. Pacific Section AAPG, Bakersfiled, CA.

Walsh MP (1983) Geochemical Flow Modeling. PhD Thesis. University of Texas, Austin, TX.